

Exciton Polariton X-waves

A. Gianfrate,¹ L. Dominici,^{1,*} O. Voronych,² M. Matuszewski,³
M. Stobińska,^{2,3,†} D. Ballarini,¹ M. De Giorgi,¹ G. Gigli,¹ and D. Sanvitto¹

¹*CNR NANOTEC, Istituto di Nanotecnologia, Via Monteroni, 73100 Lecce, Italy*

²*Institute of Theoretical Physics and Astrophysics,*

University of Gdańsk, ul. Wita Stwosza 57, 80-952 Gdańsk, Poland

³*Institute of Physics, Polish Academy of Sciences, Al. Lotników 32/46, 02-668 Warsaw, Poland*

(Dated: March 8, 2017)

In this work we experimentally demonstrate the generation of exciton-polariton X-waves and study their dynamics in time. X-waves belong to the category of localized packets, a class of states able to sustain their shape without the need of any nonlinearity. This allows to keep the packet shape for very low densities and very long times compared, for instance, to soliton waves which, on the contrary, always need nonlinearity to compensate the diffusion. The use of polaritons in microcavities is paramount since it is the unique system that allows the formation of an X-wave starting from a Gaussian spot profile. A weak four wave mixing process together with the structured non-parabolic dispersion drives the initial shaping along preferential directions that ultimately leads to the formation of a spatial X-wave front. This is the first time that such an X-wave is spontaneously generated in a 2D spatial geometry via the characteristic polariton dispersion and their nonlinearities. We also show the crucial parameters driving the phenomena, observe the redistribution by means of ultrafast imaging experiments and compare our results with numerical simulations.

POPULAR SUMMARY

Whatever platform is used if you want to transmit a signal for long distances you have to overcome two main challenges: dissipation and dispersion. Dissipation is an intrinsic characteristic of the material used, dispersion instead is something that can be manipulated by the geometry of the media and by the structure of the signal you are transmitting. Here we investigate how a non-trivial dispersion can affect the structure of the signal and its diffusion.

In this work, we excite moving wavepackets made of polaritons, hybrid two-dimensional bosonic fluid of light and matter inside a semiconductor microcavity. The mixing of photons with the electronic dipoles confers to the signal a non-parabolic dispersion. Such dispersion under opportune conditions triggers the self-resaping of the signal towards a propagation-invariant solution of the wave equation. Thanks to the coherence properties of the polaritons we can also obtain an ultrafast imaging of their fluid dynamics. We gain a fundamental understanding of the interplay of nonlinear processes and the dispersion properties, tuning them in order for the packet to assume a peculiar X-shape which is then preserved upon propagation.

Bosonic polariton X-waves can help shed light on fundamental linear and nonlinear wave dynamics and could be exploited for low intensity signal transmission in polariton based optoelectronic schemes, robust against loss-of-power distortion issues.

I. INTRODUCTION

X-waves (XWs)[1, 2] are a specific type of nonspreading wavepackets, which maintain their transverse shape along a large field-depth with respect, e.g., to Gaussian beams or packets. Another well known class of nonspreading waves, are solitons. However, in case of solitons, dispersion is constantly compensated by nonlinearity in the medium. XWs, instead, as other types of nonspreading waves, generally formed by Bessel beams, can maintain their shape also in absence of nonlinearity [3] and are relevant in any system which is governed by the wave equation. The first experimental demonstration of such optical waves employed a cw laser light [4]. These beams are not free from diffraction, but their transverse profile is such that keeps its main peak well confined, while the weaker lateral ones expand upon propagation. The same *localization* principle holds for pulsed XW packets that, in essence, are a polychromatic superposition of Bessel beams [5].

Since the early 90s XWs have been extensively studied both theoretically and experimentally using nonspreading acoustic pulses by Lu and Greenleaf [6, 7]. Later XWs were obtained with light by injecting sub-ps laser pulses across a dispersive material [3], demonstrating the potential for signal transmission and imaging. Indeed their applications span from high resolution ultrasound scanning to optical imaging, from free space communications to optical tweezers, such as accelerating or guiding beams [1]. Among their fascinating properties, it's worth mentioning that X-waves in vacuum also correspond to the simplest superluminal waveforms [8], i.e., solutions with effective velocity higher than c , which emerges from the superposition of ordinary Bessel beams [4, 5] and at the same time conform with the constraints of special relativity and the causality principle [1].

* lorenzo.dominici@gmail.com

† magdalena.stobinska@gmail.com

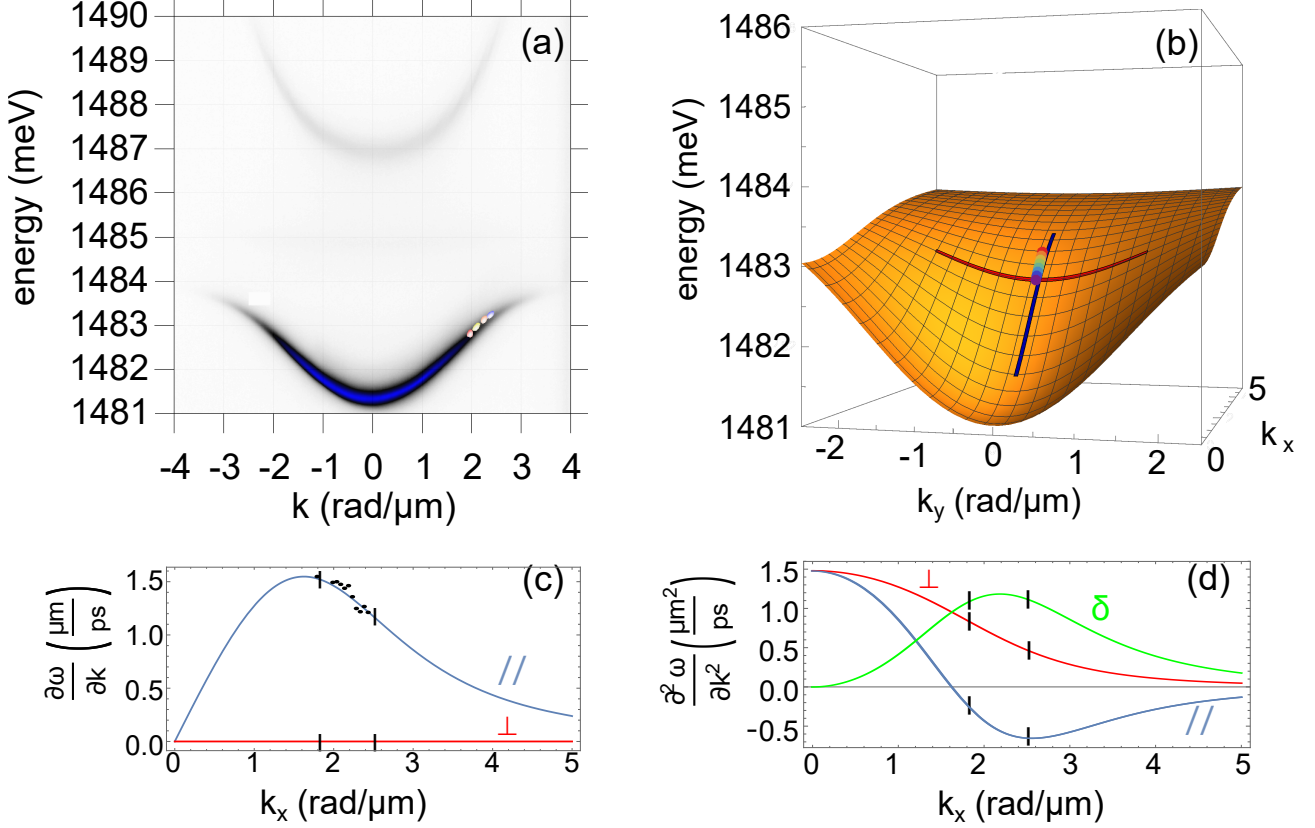


FIG. 1. (a) Experimental dispersion under non-resonant pumping. The superimposed points (different colors) on the right side of the lower branch represent polariton emission under resonant excitation at different momenta k . (b) 3D representation of the $E(k_x, k_y)$ dispersion surface around the inflection point, highlighting the central longitudinal crosscut (blue line) and an exemplificative transverse one (red line). In (c) we show the first derivative (group velocity) of the dispersion along the propagation direction (//, blue) and the transverse one (\perp , red). The black dots represent the experimental group velocities (retrieved by independent experiments on the fluid dynamics). (d) Second derivative (inverse effective mass) of the dispersion along the propagation direction (//, blue) and the transverse one (\perp , red), and their difference (δ , green). The vertical black lines define the explored k region which is maximizing the effective mass anisotropy.

The renewed interest in the XWs is also driven by their potential applicability in the field of atomic Bose-Einstein condensates (BEC) [9] and dissipative polariton condensates [10]. Both these systems bear deep similarity to the electromagnetic case because all these systems can be described by nonlinear Schrödinger equations [11]. Several theoretical proposals have been developed on the topic such as the possibility to obtain localized wave packet of matter in cold gases without needs of confining potentials [9]. Recently, a quantum description of XWs has been also developed, highlighting the difference in the entanglement properties between externally imprinted and spontaneously generated states [12]. However X-waves have not been imprinted or generated in a BEC yet.

Here we report for the first time on the experimental self-generation of an XW in a two-dimensional exciton-polariton superfluid as predicted in a recent theoretical proposal [13] following their evolution with ultra-

fast imaging. Upon fine tuning of the peculiar polariton properties we achieve a regime for self-generating an XW starting from an exciting Gaussian photonic pulse, and observe its propagation along a distance tens of μm wide.

Microcavity exciton polaritons [14–20] are bosonic particles which result from the mixing of two quasi-parabolic modes, the QW (quantum well) excitons and the MC (microcavity) photons, with dispersions of highly unbalanced curvatures. The anticrossing feature of the bare modes, associated to the strong coupling regime, finally produces the highly non-parabolic shape of one of the new normal modes, namely the lower polariton branch (LPB) [21]. In particular the presence of an inflection point, representing both a maximum of the group velocity ($v_g = \partial\omega/\partial k$) and an inversion of the so called *diffusive* effective mass [$m_{diff} = (\partial^2\omega/\partial k^2)^{-1}$] [22], is the fundamental reason for the XW spontaneous formation. Polaritons also exhibit very strong nonlineari-

ties [23, 24] able to achieve superfluid regimes [25, 26] supporting quantized vortex [27, 28], or leading to several pattern [29–32] and soliton states formation [33, 34]. However, we note that the XW, a solution which exists in the linear limit, is fundamentally different from the two-dimensional bright solitons discussed in [34, 35], where localization was achieved in the so called bistability regime, in which the soliton wavepacket was supported by an additional pump laser. These dissipative solitons exist only in a very narrow range of pumping powers and fall in the strongly nonlinear regime [35]. Differently from the case of bright solitons, that are self-sustained by nonlinear effects, polariton XW only rely on the peculiar non-parabolic dispersion, and could be exploited for the long distance propagation of signals and in new integrated optoelectronic circuits schemes.

II. EXPERIMENTS AND RESULTS

We use a high Q microcavity, the details of which can be found in Ref. [36, 37], at zero detuning between the excitonic (ψ_X) and photonic (ψ_C) fields, leading to two hybrid modes, the LPB and the upper polariton branch (UPB), well separated with respect to their linewidths. The two modes can hence manifest their dispersions, observed upon collecting the non-resonantly excited fluorescence as shown in Fig. 1(a). Here, we will focus our attention only to the LPB which shows a strong non-parabolic behavior at higher k vectors. Further experimental details can be found in the Appendix A. The 3D representation of the LPB dispersion surface $E(k_x, k_y)$ is shown in Fig. 1(b) in a region around the inflection point ($k_x \sim 1.62 \mu\text{m}^{-1}$). In the figure we highlight the non-parabolic character by reporting two orthogonal cross-cuts along the longitudinal direction (\parallel blue curve, centered at $k_y = 0$) and along the transverse direction (\perp red curve, at $k_x = 2.15 \mu\text{m}^{-1}$). The noteworthy feature that can be appreciated from the 3D representation is the opposite curvature of the two slices around the inflection point.

Moving along the central longitudinal line, the dispersion geometry always corresponds to a null transverse velocity [$\partial\omega/\partial k_y(k_x, k_y = 0)$]. The longitudinal group velocity instead grows till a maximum ($1.5 \mu\text{m}/\text{ps}$) at the inflection point and decreases for larger in-plane longitudinal momenta (k_x), Fig. 1(c). At the same time, both the longitudinal and transverse curvatures of the dispersion surface change as a function of k_x , as clearly illustrated in Fig. 1(d). In particular, the curvatures have opposite sign inside the investigated region (the explored range is denoted by dots or by vertical ticks in any of the four panels), and this corresponds to opposite effective masses.

In this work we resonantly excite the polariton superfluid by means of 2.5 ps laser pulses tuned at $\sim 836 \text{ nm}$ and focused to a $\sim 10 \mu\text{m}$ diameter spot. In Fig. 2 we show the dynamics of the effect experimentally optimized

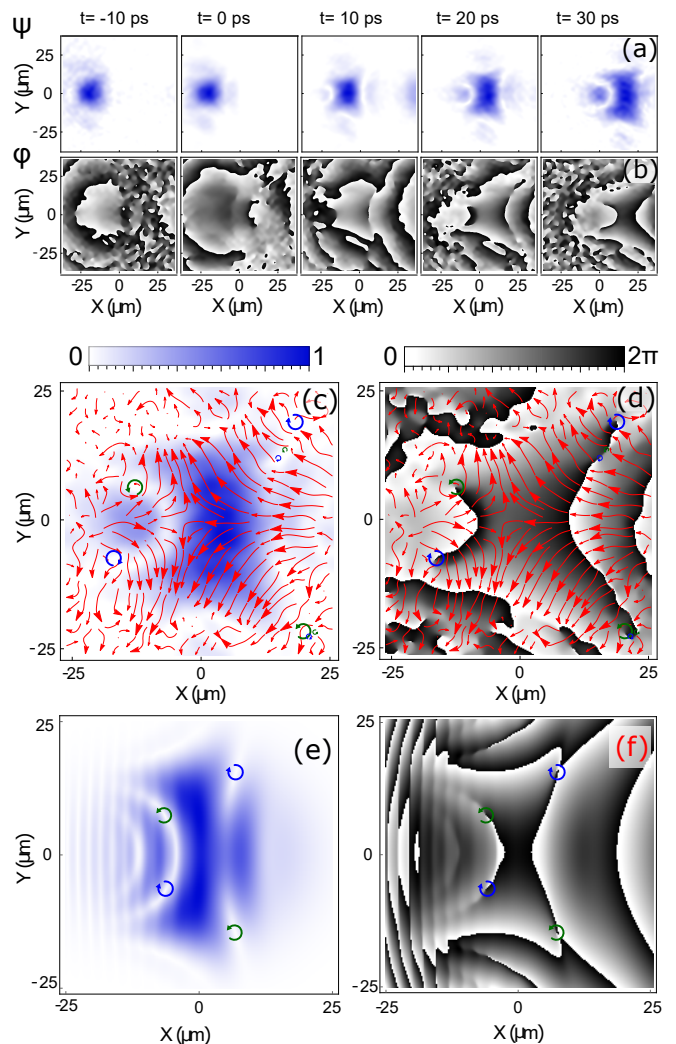


FIG. 2. Dynamical XW sequence with optimized conditions. (a,b) Spatial distribution of the polariton wavefunction (a) amplitude and (b) phase at different time frames ($t = -10, 0, 10, 20$ and 30 ps). $t = 0$ corresponds to the end of pulse injection and consequently to the start of the free evolution. The phase map is represented with respect to the moving-packets frame of reference (see also Movie 1 and 2). (c) and (d), detailed maps of the amplitude and phase ($t = 27.5$ ps), with superposition of the relative in-plane momenta distribution (red arrows) and of the quantized vortices (blue and green circles). (e) and (f) GPE simulated amplitude and phase maps at 27.5 ps for a $10 \mu\text{m}$ wide pump spot and a wavevector of $2.55 \mu\text{m}^{-1}$.

using $k = 2.35 \mu\text{m}^{-1}$ and $75 \mu\text{W}$ pumping power. Figure 2(a) displays the modulus and Fig. 2(b) the phase of the polariton X-wavepacket. The time zero in the temporal evolution is set when the pump stops injecting polaritons and these are left free to evolve within their lifetime. Initially, the density distribution reveals a Gaussian shape with a rather homogeneous phase (with just a weak radial gradient associated to the beam curvature). However, after 10 ps the X-shape can be already neatly dis-

tinguished. At the successive $t = 20$ ps and $t = 30$ ps snapshots, we can appreciate just a small vertical spread of the packet, however without a significant distortion in the shape. Noticeably, the longitudinal waist remains fundamentally constant, despite the polariton lifetime is ~ 10 ps [36, 37].

A very interesting feature can be spotted in the phase map, as shown in Fig. 2(b): the appearance of four quantized vortices, at the edges of the packet. Such vortex pairs are very well associated to the driving in-plane momenta and fluxes. They are shown in detail in the maps of Fig. 2(c,d), overlapping the streamlines of the phase gradient (red arrows) and the dots of the phase singularities (blue and green arrow circles). The hyperbolic feature of the flux, pushing the polaritons inward along the propagation direction, consequently keeping the signal compact, and outward in the transverse direction, is strong in the center of the packet.

The dynamics of the polariton superfluid was successfully modeled within the mean field approximation, by a set of coupled equations equivalent to the Gross-Pitaevskii equation (GPE):

$$\begin{cases} i\hbar \frac{d}{dt} \psi_C = \frac{\Omega_R}{2} \psi_X + \left(\frac{\hbar\gamma_C}{2i} - \frac{\hbar^2}{2m_C} \partial_x^2 - \frac{\hbar^2}{2m_C} \partial_y^2 \right) \psi_C, \\ i\hbar \frac{d}{dt} \psi_X = \frac{\Omega_R}{2} \psi_C + \left(\frac{\hbar\gamma_X}{2i} + g|\psi_X|^2 \right) \psi_X, \end{cases} \quad (1)$$

where m_C is the effective mass of microcavity photons, Ω_R is the Rabi frequency coupling the photonic ψ_C and excitonic ψ_X fields, γ_C and γ_X are the associated decay rates and g is the nonlinear interaction term in the exciton component. Further details are given in Appendix B. The results shown in Fig. 2(e,f) represent the amplitude and phase maps, respectively, at a time of 27.5 ps, demonstrating a very good agreement with the main experimental features. The modulation in the tail of the signal that can be spotted in the theoretical Fig. 2(e,f) could be due to the interference with a weak nonlinear scattering to opposite k_x states. This may be not visible in the experimental data due to the temporal resolution (2.5 ps limited by the reference pulse).

The opposite transverse and longitudinal effective masses confer to the GPE—that describes the polariton dynamics—a highly hyperbolic character. This behavior is crucial to sustain the X-wave phenomena, and demonstrates that the shape conservation does not rely on the nonlinearity as in the case of solitons [30, 34], but rather on the dispersion morphology. It was previously shown that an X-shaped initial profile can be a stationary solution of the linear GPE model [13]. We experimentally demonstrate that in a weakly nonlinear regime, an initial Gaussian state can be triggered to spontaneously evolve into a steady X-wave via an early FWM (Four Wave Mixing) process. In the dynamics it is possible to qualitatively distinguish three main different phases: pulse injection ($-5 \div 0$ ps), initial redistribution ($0 \div 10$ ps), propagation ($10 \div 30$ ps).

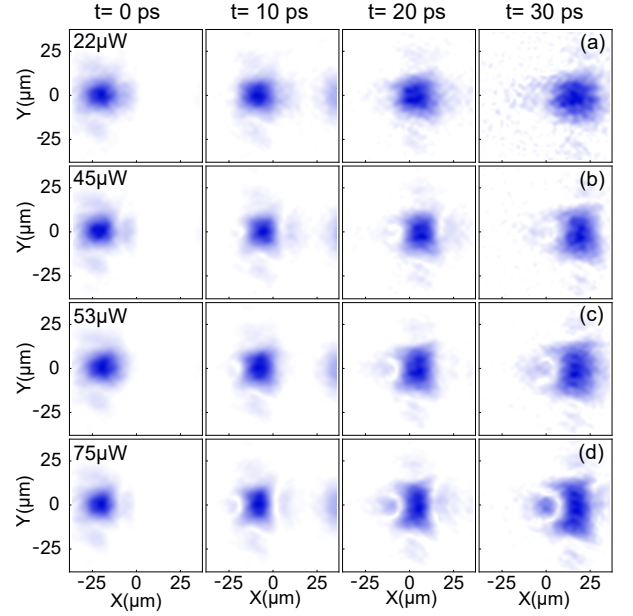


FIG. 3. Packet reshaping and propagation under the effect of different pumping powers. In (a,b,c,d) each row is relevant to a different power and the same optimum injection wavevector ($k_x = 2.35 \mu\text{m}^{-1}$).

III. INTERPLAY OF NONLINEARITY AND NON-PARABOLIC DISPERSION

Although the nonlinearities have no role in the propagation and sustain of the signal, they are crucial for the initial reshaping of the Gaussian pulse, which is the triggering of the X-packet. Indeed the choice of the initial spot size itself in real space (density FWHM $\sim 10 \mu\text{m}$) is set to achieve a proper extension in the reciprocal (momentum) space (FWHM $\sim 0.6 \mu\text{m}^{-1}$), and exploit the negative curvature. The nonlinearity is needed to allow an asymmetric momentum redistribution according dispersion shape. The overall result is an elongated spot in the reciprocal k space along the direction of propagation, associated to stronger confinement in real space.

To highlight the effect of the nonlinearities the temporal dynamics at four different pumping powers are shown in Fig. 3. At low density, Fig. 3(a), the reshaping is absent and the signal spreads uniformly in both directions, longitudinal and transverse to the propagation. However, increasing the pump power the intensity redistribution anisotropy between the longitudinal and transverse diffusion starts to appear as shown in Fig. 3(b,c). At $75 \mu\text{W}$ the reshaping reaches its optimum, Fig. 3(d), and the packet shows a very well defined X-shape, together with a small circular tail. Above this power the dynamics enter a strongly nonlinear regime (between $100 \mu\text{W}$ and $500 \mu\text{W}$), where the redistribution due to the high densities involve radial counterflows which reshape the signal beyond a recognizable X-packet. Such regime is

just before the onset of the dynamical nonlinearity inversion leading to the real space collapse described in [30].

The role played by the in-plane momentum k_x is shown in Fig. 4 where only the injection angle is changed while keeping constant the initial density. In Fig. 4(a), despite that the nonlinearities are of same amount as those in Fig. 3(d), no redistribution is observed. Upon gradually increasing the injection angle, Fig. 4(b) and (c), the packet shows again a marked anisotropy in the diffusion along the longitudinal and transverse direction. This is due to the larger difference between the longitudinal and transverse effective masses in the excited region of the dispersion. This difference reaches its maximum at $2.35 \mu\text{m}^{-1}$ where the reshaping is finally optimized, Fig. 4(d).

We now focus on the dynamics of the polariton XWs. Figure 5(a) shows the time evolution of the normalized polariton population (blue points) together with the pump pulse temporal envelope (solid red curve). The $t = 0$ ps has been chosen at the maximum of the polariton population, when the pulse has essentially finished its pumping action and the polaritons free evolution starts. The growing longitudinal/transverse anisotropy can be appreciated upon a visual comparison between the associated timespace charts in Fig. 5(b) (longitudinal) and Fig. 5(c) (transverse). In the former the signal propagates for $40 \mu\text{m}$ with a constant speed of $\sim 1.33 \mu\text{m}/\text{ps}$, with a final longitudinal width very much the same as the original shape, while in the latter the transverse width reveals instead a standard wave-packet diffusion. This is clearly shown in Fig. 5(d,e), where both the longi-

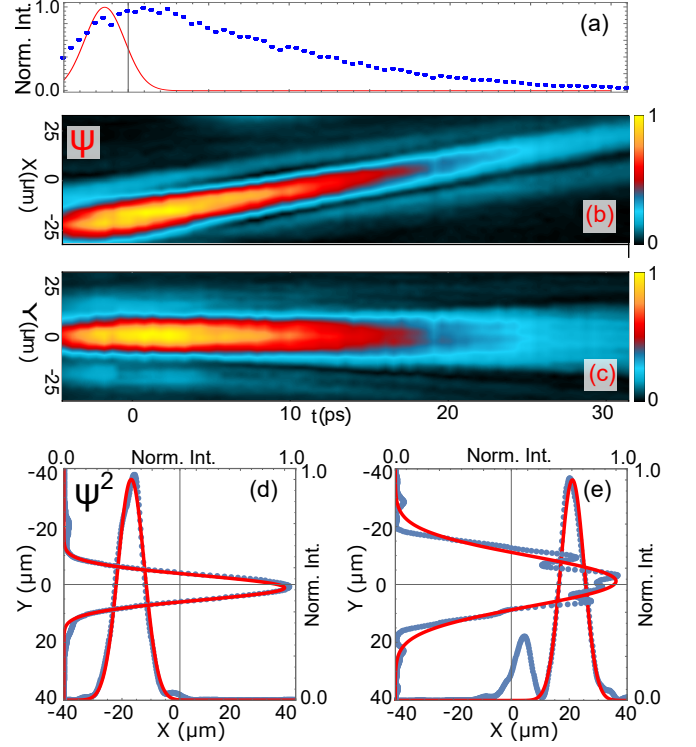


FIG. 5. (a) In blue, time evolution of the normalized total polariton population, in red the temporal envelope of the pump pulse. (b,c) Vertical and horizontal timespace charts for $P = 75 \mu\text{W}$, $k_x = 2.35 \mu\text{m}^{-1}$. The transverse crosscuts in (b,c) are taken at a longitudinal position which follows the packet maximum. (d,e) Longitudinal and transverse normalized density profiles for $P = 75 \mu\text{W}$ at $t = 0$ ps (d) and $t = 30$ ps (e). Solid lines are Gaussian fits.

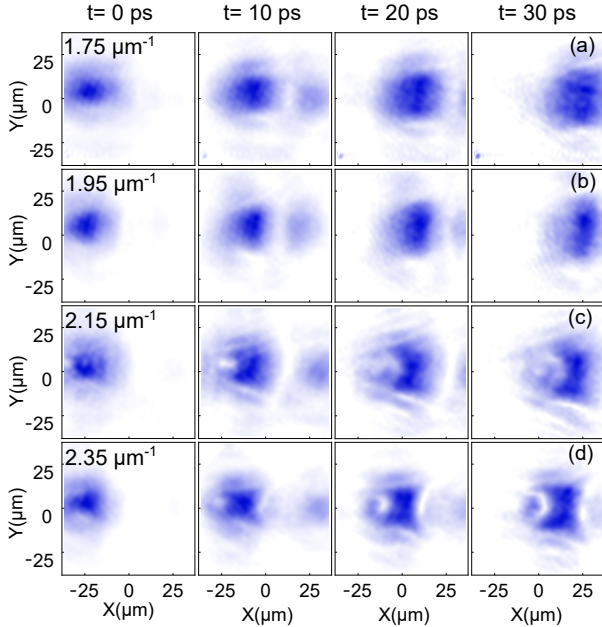


FIG. 4. Packet reshaping and propagation for different in plane wave-vector. In (a,b,c,d) the pumping power is kept constant ($80 \mu\text{W}$) while the in plane momentum is changed.

tudinal and transverse profiles are reported for $t = 0$ and $t = 30$ ps, respectively, together with the associated Gaussian fits.

The power dependence of the differential spreading along the two directions is analyzed in detail in Fig. 6(a). Here the temporal evolution of the longitudinal and transverse density FWHMs is shown for different excitation powers, corresponding to the previous Fig. 3(a-d). For the lowest power ($P = 22 \mu\text{W}$, red line), the reshaping is completely absent and the wavepacket expands continuously in both directions, longitudinal (filled dots) and transverse (open dots) with the same spreading rate. At larger injected power, and consequently stronger nonlinearity, there is an anisotropic evolution between the longitudinal and transverse widths which gradually increases ($P = 45 \mu\text{W}$, $P = 53 \mu\text{W}$, orange and green dots, respectively). Finally, for $P = 75 \mu\text{W}$ when the X-shape can be clearly distinguished in the previous maps of Fig. 3(d), the longitudinal spreading is suppressed while the transverse size continues to grow. For the highest power the longitudinal squeezing in the first 10 ps is associated to the initial redistribution into the X-wave packet caused by the nonlinearities. Figure 6(b) shows

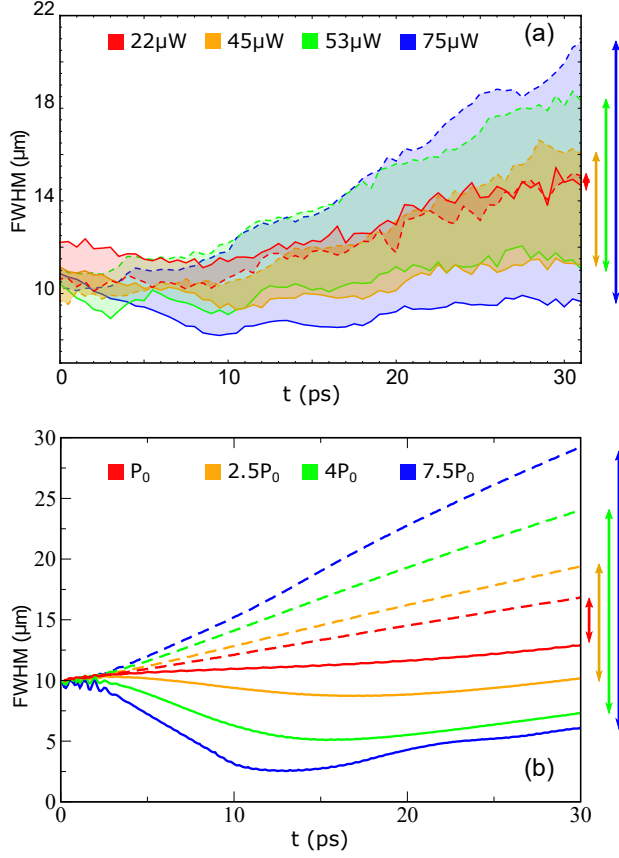


FIG. 6. (a) Experimental longitudinal (solid line) and transverse (dashed line) density FWHMs during time at four different excitation powers for $k_x = 2.35 \mu\text{m}^{-1}$. (b) Simulation of the time evolution of the longitudinal (solid line) and transverse (dashed line) density FWHMs, for different initial total populations and $k_x = 2.55 \mu\text{m}^{-1}$ in-plane momentum. The arrows on the right side in both panels indicate the difference between the longitudinal and transverse widths.

the numerical simulations reproducing the experiments in a perfect agreement with our trends.

As introduced in the previous Fig. 2, a specific feature of our structured polariton XW is represented by the leading and trailing islands which are developed around the main packet during the initial reshaping. In Fig. 7(a) we report both the density and phase longitudinal profiles (corresponding to $P = 75 \mu\text{W}$ and $t = 7.5 \text{ ps}$) to highlight the presence of two sharp π -jumps in front and behind the main packet. These features are indicating nonlinear interference phenomena between counter propagating flows. In general, the nonlinear self-development of a π -jump may be a signature of a dark soliton [30, 38], which can be sustained in two-dimensional condensates upon repulsive interactions [39]. In Fig. 7(b) we report the evolution of the phase profiles at equidistant time frames (every 2.5 ps). The profiles evidence how the sharp π -jump is only present in a given frame at early times, before smoothing down as expected due to the

loss of intensity. Hence we may conclude that the dark soliton is just a transient structure here, formed thanks to the nonlinear way we obtain the XW in the polariton fluid and is then washed out, without representing an intrinsic feature of the XW itself at longer times.

IV. CONCLUSIONS

We experimentally demonstrated the possibility to excite a peculiar class of traveling localized wavepackets, called X-waves, in two-dimensional exciton-polariton fluids. The self-generation of an X-wave out of a Gaussian excitation spot is obtained via a weakly nonlinear process taking place asymmetrically along the two directions of the non-parabolic polariton dispersion. We have investigated the proper tuning of both the nonlinearity and the injected in-plane momentum in order to achieve an optimal effect. The dynamics of the packet are observed by means of ultrafast imaging, revealing a propagation over tens of micrometers, only limited by the polariton dissipation. Two-dimensional X-wavepackets are devised as robust signal carrier candidates for polariton based all-optical platforms.

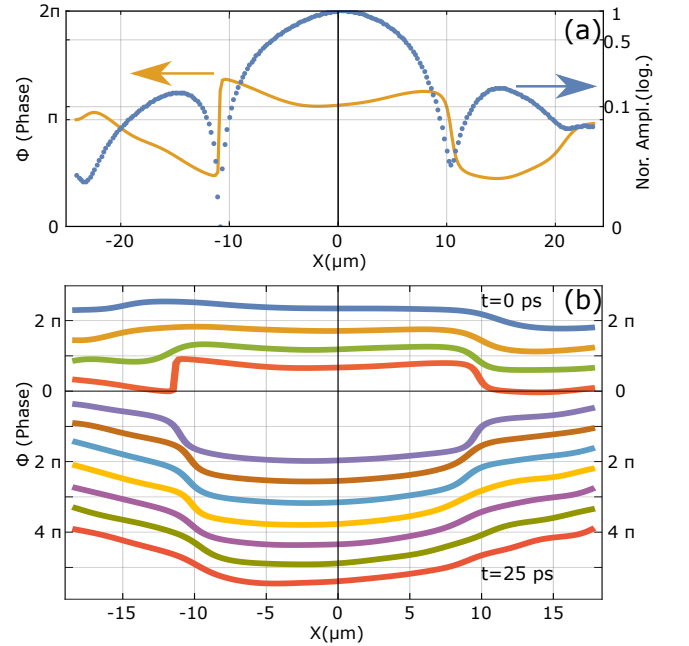


FIG. 7. (a) Phase (solid orange line) and amplitude (blue dots) central crosscut profiles along the propagation direction, at $t = 7.5 \text{ ps}$ and for $P = 75 \mu\text{W}$. (b) Phase profiles along the longitudinal axis at fixed time intervals of 2.5 ps. The top line represents $t = 0 \text{ ps}$ while the subsequent profiles are mutually shifted downward of the same amount for the clarity of representation.

ACKNOWLEDGMENTS

We thank R. Houdré and A. Bramati for the growth expertise of the microcavity device. AG, LD, DB, MDG, GG and DS are supported by the European Research Council POLAFLOW Grant 308136 and the Italian MIUR project Beyond Nano. MS and OV are supported by the NCN grant No. 2012/04/M/ST2/00789 and MNiSW Iuventus Plus project No. IP 2014 044873. MM acknowledges support from the NCN grant 2015/17/B/ST3/02273.

APPENDIX A: EXPERIMENTAL METHODS

The experiments described here are performed on a GaAs/Al_xGaAs microcavity (MC) composed by three quantum wells (QW) enclosed by two distributed Bragg reflectors. The positions inside the MC are set in order to have the QWs in the antinodes of the confined photonic field. This sample is also grown on a specific doped GaAs substrate with a transparency window centered at 830 nm, that consequently allows to work in a transmission configuration. The sample is kept at a constant temperature of 10 K by means of a cryostat avoiding thermal ionization of excitons.

The setup in use during this experiment is an ultrafast digital holography setup described in detail in Ref. [36, 37], where the emission signal is let interfere with a homodyne uniform plane wave reference. The two beams are sent with a slightly different incidence angle on a charge coupled device camera to collect the associated interference pattern. The resulting interferograms are analyzed by a digital Fast Fourier Transformation to obtain the amplitude (ψ) and the phase (φ) of the complex wavefunction in real space. A delay line on the reference optical path allows us to scan the signal in time upon changing the time delay of the reference. The temporal resolution of this technique is mainly limited by the duration of the picosecond laser pulse in use, 2.5 ps, which

in the current experiments allows to selectively excite the lower polariton mode upon proper tuning at ~ 836 nm. The time step was set to 0.5 ps.

Circular polarization is set in the excitation beam in order to generate only one spin population and consequently maximize the interactions. The same reshaping effects are obtained upon a double total population density when using a linearly polarized excitation beam. The pump spot is set to a $\text{FWHM}_{x,y} = 10 \mu\text{m}$ ($\text{FWHM}_{k_x,k_y} = 0.6 \mu\text{m}^{-1}$ in the reciprocal space), in order to facilitate the nonlinear scattering process in real space and have a wide enough spot to cover the interested dispersion range in k space.

APPENDIX B: NUMERICAL METHODS

To illustrate the dynamical X-wave formation and localization induced by the nonlinearity, we performed simulations starting from a Gaussian initial state $\Psi(x, y) = \frac{1}{\sqrt{2\pi\sigma^2}} \exp\{-(x^2 + y^2)/(2\sigma^2)\}$ where $\sigma = \text{FWHM}/(2\sqrt{2\ln 2})$ and FWHM is the full width at half-maximum of the Gaussian spot. The GPE described in the text was solved numerically using the Runge-Kutta method of 4th order. The device parameters were: $m_C = 4.27 \times 10^{-5} m_e$, $\gamma_C = 0.2 \text{ ps}^{-1}$, $\gamma_X = 0.2 \text{ ps}^{-1}$, $g = 2 \times 10^{-3} \text{ meV} \cdot \mu\text{m}^2$, $\delta = -0.55 \text{ meV}$, $\Omega_R = 5.4 \text{ meV}$. The details of the numerical method are described in [10]. Numerical computations were performed with Zeus cluster of the ACK “Cyfronet” AGH computer center.

APPENDIX C: SUPPLEMENTARY MOVIES

Supplementary Movie S1: Dynamical X-wave experiment as described in Fig. 2. The time step is 0.5 ps.

Supplementary Movie S2: 3D representation of the amplitude dynamics in the X-wave experiment of Fig. 2.

-
- [1] E. Recami, M. Zamboni-Rached, H. E. Hernández-Figueroa, Localized Waves: A scientific and historical introduction, in *Localized waves*, Wiley series in microwave and optical engineering, edited by H. E. Hernández-Figueroa, M. Zamboni-Rached, E. Recami (Wiley-Interscience : IEEE Press, Hoboken, N.J, 2008) Chap. 1, pp. 1–41.
 - [2] E. Recami, M. Zamboni-Rached, Localized Waves: A Review, in *Advances in Imaging and Electron Physics*, Vol. 156 (Elsevier, 2009) Chap. 4, pp. 235–353.
 - [3] H. Sönajalg, M. Rätsep, P. Saari, *Demonstration of the Bessel-X pulse propagating with strong lateral and longitudinal localization in a dispersive medium*, Opt. Lett. **22**, 310 (1997).
 - [4] J. Durnin, J. J. Miceli, J. H. Eberly, *Diffraction-free beams*, Phys. Rev. Lett. **58**, 1499 (1987).
 - [5] J. Salo, J. Fagerholm, A. T. Friberg, M. M. Salomaa, *Unified description of nondiffracting X and Y waves*, Phys. Rev. E **62**, 4261 (2000).
 - [6] J. Y. Lu, J. F. Greenleaf, *Ultrasonic nondiffracting transducer for medical imaging*, IEEE Trans. Ultrason. Ferroelect. Freq. Control **37**, 438 (1990).
 - [7] J. Y. Lu, J. F. Greenleaf, *Nondiffracting X waves-exact solutions to free-space scalar wave equation and their finite aperture realizations*, IEEE Trans. Ultrason. Ferroelect. Freq. Control **39**, 19 (1992).
 - [8] M. Zamboni-Rached, E. Recami, H. Hernández-Figueroa, *New localized Superluminal solutions to the wave equations with finite total energies and arbitrary frequencies*,

- Eur. Phys. J. D **21**, 217 (2002).
- [9] C. Conti, S. Trillo, *Nonspreading Wave Packets in Three Dimensions Formed by an Ultracold Bose Gas in an Optical Lattice*, Phys. Rev. Lett. **92**, 120404 (2004).
 - [10] O. Voronich, A. Buraczewski, M. Matuszewski, M. Stobińska, *Numerical modeling of exciton-polariton Bose-Einstein condensate in a microcavity*, Comput. Phys. Commun., in press (2017).
 - [11] N. K. Efremidis, G. A. Siviloglou, D. N. Christodoulides, *Exact X-wave solutions of the hyperbolic nonlinear Schrödinger equation with a supporting potential*, Phys. Lett. A **373**, 4073 (2009).
 - [12] A. Ciattoni, C. Conti, *Quantum electromagnetic X waves*, J. Opt. Soc. Am. B **24**, 2195 (2007).
 - [13] O. Voronich, A. Buraczewski, M. Matuszewski, M. Stobińska, *Exciton-polariton localized wave packets in a microcavity*, Phys. Rev. B **93**, 245310 (2016).
 - [14] D. Sanvitto, S. Kéna-Cohen, *The road towards polaritonic devices*, Nat. Mater. **15**, 1061 (2016).
 - [15] T. Byrnes, N. Y. Kim, Y. Yamamoto, *Exciton-polariton condensates*, Nat. Phys. **10**, 803 (2014).
 - [16] G. Dagvadorj, J. M. Fellows, S. Matyjaśkiewicz, F. M. Marchetti, I. Carusotto, M. H. Szymańska, *Nonequilibrium Phase Transition in a Two-Dimensional Driven Open Quantum System*, Phys. Rev. X **5**, 041028 (2015).
 - [17] H. Deng, H. Haug, Y. Yamamoto, *Exciton-polariton Bose-Einstein condensation*, Rev. Mod. Phys. **82**, 1489 (2010).
 - [18] A. Amo, D. Sanvitto, F. P. Laussy, D. Ballarini, E. d. Valle, M. D. Martin, A. Lemaître, J. Bloch, D. N. Krizhanovskii, M. S. Skolnick, C. Tejedor, L. Viña, *Collective fluid dynamics of a polariton condensate in a semiconductor microcavity*, Nature **457**, 291 (2009).
 - [19] J. Kasprzak, M. Richard, S. Kundermann, A. Baas, P. Jeambrun, J. M. J. Keeling, F. M. Marchetti, M. H. Szymańska, R. André, J. L. Staehli, V. Savona, P. B. Littlewood, B. Deveaud, L. S. Dang, *Bose-Einstein condensation of exciton polaritons*, Nature **443**, 409 (2006).
 - [20] R. Balili, V. Hartwell, D. Snoke, L. Pfeiffer, K. West, *Bose-Einstein Condensation of Microcavity Polaritons in a Trap*, Science **316**, 1007 (2007).
 - [21] A. V. Kavokin, J. J. Baumberg, G. Malpuech, F. P. Laussy, *Microcavities*, 2nd ed., Series on Semiconductor Science and Technology (Oxford University Press, Oxford, New York, 2017).
 - [22] D. Colas, F. P. Laussy, *Self-Interfering Wave Packets*, Phys. Rev. Lett. **116**, 026401 (2016).
 - [23] P. M. Walker, L. Tinkler, D. V. Skryabin, A. Yulin, B. Royall, I. Farrer, D. A. Ritchie, M. S. Skolnick, D. N. Krizhanovskii, *Ultra-low-power hybrid light-matter solitons*, Nat. Commun. **6**, 8317 (2015).
 - [24] M. Vladimirova, S. Cronenberger, D. Scalbert, K. V. Kavokin, A. Miard, A. Lemaître, J. Bloch, D. Solnyshkov, G. Malpuech, A. V. Kavokin, *Polariton-polariton interaction constants in microcavities*, Phys. Rev. B **82**, 075301 (2010).
 - [25] A. Amo, J. Lefrère, S. Pigeon, C. Adrados, C. Ciuti, I. Carusotto, R. Houdré, E. Giacobino, A. Bramati, *Superfluidity of polaritons in semiconductor microcavities*, Nat. Phys. **5**, 805 (2009).
 - [26] A. C. Berceanu, L. Dominici, I. Carusotto, D. Ballarini, E. Cancellieri, G. Gigli, M. H. Szymańska, D. Sanvitto, F. M. Marchetti, *Multicomponent polariton superfluidity in the optical parametric oscillator regime*, Phys. Rev. B **92**, 035307 (2015).
 - [27] A. Amo, S. Pigeon, D. Sanvitto, V. G. Sala, R. Hivet, I. Carusotto, F. Pisanello, G. Lemenager, R. Houdré, E. Giacobino, C. Ciuti, A. Bramati, *Polariton Superfluids Reveal Quantum Hydrodynamic Solitons*, Science **332**, 1167 (2011).
 - [28] D. Sanvitto, F. M. Marchetti, M. H. Szymańska, G. Tosi, M. Baudisch, F. P. Laussy, D. N. Krizhanovskii, M. S. Skolnick, L. Marrucci, A. Lemaître, J. Bloch, C. Tejedor, L. Viña, *Persistent currents and quantized vortices in a polariton superfluid*, Nat. Phys. **6**, 527 (2010).
 - [29] C. E. Whittaker, B. Dzurak, O. A. Egorov, G. Buonaiuto, P. M. Walker, E. Cancellieri, D. M. Whittaker, E. Clarke, S. S. Gavrilov, M. S. Skolnick, D. N. Krizhanovskii, *Polariton pattern formation and its statistical properties in a semiconductor microcavity*, arXiv:1612.03048 [cond-mat] (2016).
 - [30] L. Dominici, M. Petrov, M. Matuszewski, D. Ballarini, M. D. Giorgi, D. Colas, E. Cancellieri, B. S. Fernández, A. Bramati, G. Gigli, A. Kavokin, F. Laussy, D. Sanvitto, *Real-space collapse of a polariton condensate*, Nat. Commun. **6**, 8993 (2015).
 - [31] F. Manni, K. G. Lagoudakis, T. C. H. Liew, R. André, B. Deveaud-Plédran, *Spontaneous Pattern Formation in a Polariton Condensate*, Phys. Rev. Lett. **107**, 106401 (2011).
 - [32] E. Wertz, L. Ferrier, D. D. Solnyshkov, R. Johné, D. Sanvitto, A. Lemaître, I. Sagnes, R. Grousson, A. V. Kavokin, P. Senellart, G. Malpuech, J. Bloch, *Spontaneous formation and optical manipulation of extended polariton condensates*, Nat. Phys. **6**, 860 (2010).
 - [33] E. A. Ostrovskaya, J. Abdullaev, A. S. Desyatnikov, M. D. Fraser, Y. S. Kivshar, *Dissipative solitons and vortices in polariton Bose-Einstein condensates*, Phys. Rev. A **86**, 013636 (2012).
 - [34] M. Sich, D. N. Krizhanovskii, M. S. Skolnick, A. V. Gorbach, R. Hartley, D. V. Skryabin, E. A. Cerda-Méndez, K. Biermann, R. Hey, P. V. Santos, *Observation of bright polariton solitons in a semiconductor microcavity*, Nat. Photon. **6**, 50 (2012).
 - [35] O. A. Egorov, A. V. Gorbach, F. Lederer, D. V. Skryabin, *Two-Dimensional Localization of Exciton Polaritons in Microcavities*, Phys. Rev. Lett. **105**, 073903 (2010).
 - [36] D. Colas, L. Dominici, S. Donati, A. A. Pervishko, T. C. Liew, I. A. Shelykh, D. Ballarini, M. de Giorgi, A. Bramati, G. Gigli, E. d. Valle, F. P. Laussy, A. V. Kavokin, D. Sanvitto, *Polarization shaping of Poincaré beams by polariton oscillations*, Light Sci. Appl. **4**, e350 (2015).
 - [37] L. Dominici, D. Colas, S. Donati, J. P. Restrepo Cuartas, M. De Giorgi, D. Ballarini, G. Guirales, J. C. López Carreño, A. Bramati, G. Gigli, E. del Valle, F. P. Laussy, D. Sanvitto, *Ultrafast Control and Rabi Oscillations of Polaritons*, Phys. Rev. Lett. **113**, 226401 (2014).
 - [38] L. Dominici, G. Dagvadorj, J. M. Fellows, D. Ballarini, M. De Giorgi, F. M. Marchetti, B. Piccirillo, L. Marrucci, A. Bramati, G. Gigli, M. H. Szymańska, D. Sanvitto, *Vortex and half-vortex dynamics in a nonlinear spinor quantum fluid*, Sci. Adv. **1**, e1500807 (2015).
 - [39] A. S. Rodrigues, P. G. Kevrekidis, R. Carretero-González, J. Cuevas-Maraver, D. J. Frantzeskakis, F. Palmero, *From nodeless clouds and vortices to gray ring solitons and symmetry-broken states in two-dimensional polariton condensates*, J. Phys.: Condens. Matter **26**, 155801 (2014).